Journal of Medicinal Chemistry

Article

pubs.acs.org/jmc

Optimization of Potent *DFG-in* Inhibitors of Platelet Derived Growth Factor Receptorβ (PDGF-Rβ) Guided by Water Thermodynamics

Rebecca Horbert,[†,∥] Boris Pinchuk,[†,∥] Eugen Johannes,[†] Joachim Schlosser,[†] Dorian Schmidt,[†] Daniel Cappel,[‡] Frank Totzke,[§] Christoph Schächtele,[§] and Christian Peifer*[,†]

[†]Institute of Pharmacy, Christian-Albrechts-University of Kiel, Gutenbergstraße 76, D-24116 Kiel, Germany

[‡]Schrödinger GmbH, Dynamostraße 13, D-68165 Mannheim, Germany

[§]ProQinase GmbH, Breisacherstraße 117, D-79106 Freiburg, Germany

Supporting Information

ABSTRACT: In this study we report on the hit optimization of substituted 3,5-diaryl-pyrazin-2(1*H*)-ones toward potent and effective platelet-derived growth factor receptor (PDGF-R) β-inhibitors. Originally, the 3,5-diaryl-pyrazin-2-one core was derived from the marine sponge alkaloid family of hamacanthins. In our first series compound **2** was discovered as a promising hit showing strong activity against PDGF-Rβ in the kinase assay (IC_{50} = 0.5 μM). Furthermore, **2** was shown to be selective for PDGF-Rβ in a panel of 24 therapeutically relevant protein kinases. Molecular modeling studies on a PDGF-Rβ homology model using prediction of water thermodynamics suggested an optimization strategy for the 3,5-diaryl-pyrazin-2-ones as *DFG-in* binders by using a phenolic OH function to replace a structural water molecule in the ATP binding site. Indeed, we identified compound **38** as a highly potent inhibitor with an IC_{50} value of 0.02 μM in a PDGF-Rβ enzymatic assay also showing activity against PDGF-R dependent cancer cells.

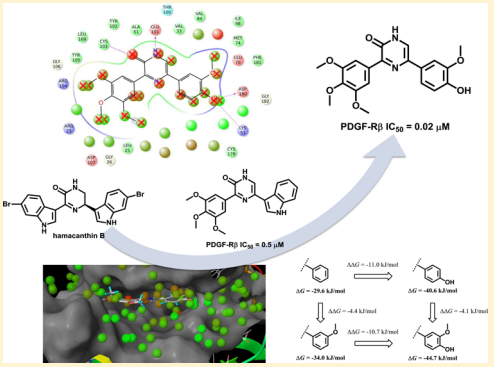

INTRODUCTION

In our ongoing study to develop ATP-competitive receptor tyrosine kinase (RTK) inhibitors with anticancer activity, we focused on the hamacanthin B family of deep-sea sponge derived bis-indole alkaloids possessing a 3,5-bisindole-3,4-dihydropyrazin(1*H*)-2-one scaffold.[1] In line with this notion, *cis*-3,4-dihydropyrazin(1*H*)-2-one hamacanthin B was reported to be a potent bacterial methicillin-resistant *Staphylococcus* protein kinase inhibitor (MRSA-PK inhibitor) with an IC_{50} value of 0.016 μM and possessing significant selectivity over human protein kinase isoforms.[2] Moreover, substituted (1*H*)-pyrazin-2-ones have been investigated as human protein kinase (PK) inhibitors showing this moiety to be suitable as a core scaffold for PK inhibitor design.[3] Among human PKs in oncology, overactivated RTK including VEGFR, PDGF-R, and c-kit are considered to be major targets for the development of clinically effective inhibitors.[4] Thus, many anticancer compounds that are advanced into the clinic show (group-) selectivity toward VEGF-R, FGF-R, EGF-R, PDGF-R, c-kit, and Flt-3 (Chart 1).[5] Furthermore, inhibitors addressing a single PK with high selectivity are of significant interest. A recent study reported about the development of imidazo[1,2-α]pyridines with potent PDGF-R activity and oral bioavailability.[6]

Therefore, we designed the aryl-substitution patterns of the 6-membered 3,5-diaryl-pyrazin-2(1*H*)-one **2**[1] based on the corresponding 5-membered 3,4-diaryl-2*H*-pyrrole-2-one (compound **1**, Chart 2), a potent inhibitor of VEGF-R2/3 (IC_{50} = 0.03 μM) with good efficacy in cellular assays.[7]

RESULTS AND DISCUSSION

Chemistry. The test compounds reported in this study were synthesized by our flexible synthetic platform to produce targeted 3,5-diaryl-pyrazin-2(1*H*)-ones (VI, Scheme 1).[8] As key intermediates for the final ring closure, the open-chained diketoamides (V) were accessible via two different routes. On the one hand, arylglyoxylic acid (I) was activated by carbonyldiimidazole (CDI) and coupled with the α-ketoamine moiety (II) to produce the open-chained diketoamide (V). On the other hand, CDI mediated coupling of arylglyoxylic acid (I) and amine (III) gave amide (IV), which yielded ketoamide (V) upon DDQ-oxidation. Microwave-mediated ring closure in the final step by using the open-chained diketoamide (V) and ammonium acetate as nitrogen source yielded the desired 3,5-diaryl-pyrazin-2(1*H*)-ones (VI).

Molecular Modeling and Binding Mode. In a preliminary *in vitro* screening involving 24 therapeutically relevant PK, compound **2** was actually determined to potently inhibit PDGF-Rβ with an IC_{50} of 0.5 μM.[1] Moreover, compound **2** was shown to be selective over the other PK enzymes tested in

Special Issue: New Frontiers in Kinases

Received: March 10, 2014

   dx.doi.org/10.1021/jm500373x | J. Med. Chem. XXXX, XXX, XXX−XXX

Chart 1. Selection of Small Molecule Kinase Inhibitors (smKI, Approved or in Clinical Phases) Targeting PDGF-R (among Other PKs)

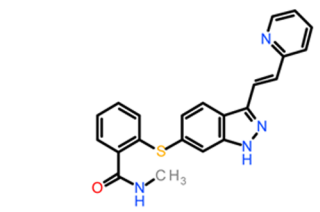
Axitinib

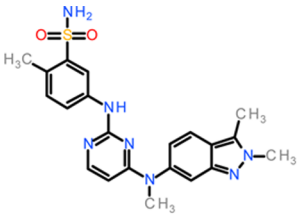
Pazopanib

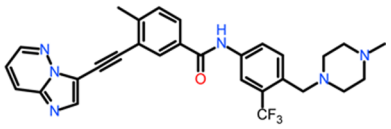
Ponatinib

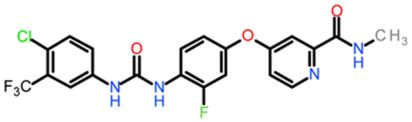
Regorafenib

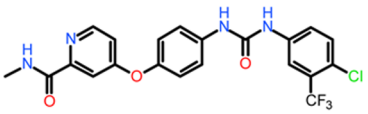
Sorafenib

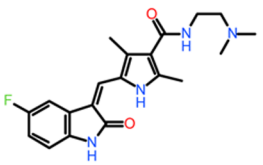
Sunitinib

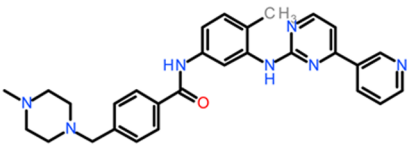
Imatinib

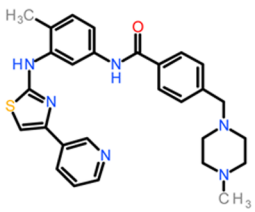
Masitinib

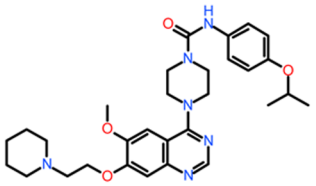
Tandutinib

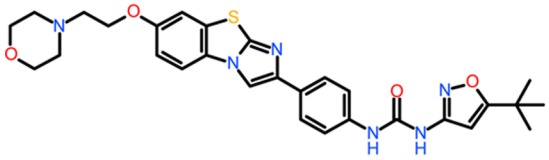
Quizartinib

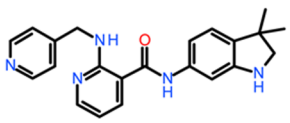
Motesanib

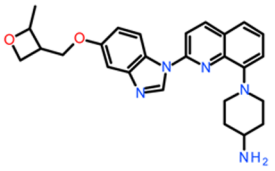
Crenolanib

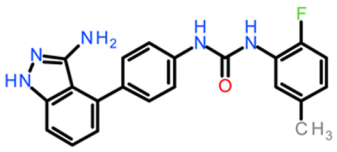
Linifanib

this panel (VEGF-R2 IC_{50} = 4 μM, VEGF-R3 IC_{50} = 5 μM, FLT3 IC_{50} = 36 μM; IC_{50}-values >100 μM: AKT1, ARK5, Aurora-A/B, B-RAF-VE, CDK2/CycA, CDK4/CycD1, COT, EGFR, EPHB4, ERBB2, FAK, IGF1R, SRC, INSR, MET, PLK1, SAK, TIE2, and CK2a1). Thus, we aimed to further enhance the potency of this hit compound toward PDGF-Rβ by using a homology model/docking approach since no X-ray structure of the PDGF-R PK domain is available in the public domain. Besides, the vast majority of ATP-competitive inhibitors can be categorized in type I or type II binders.[9] That is, binding two different conformations of the ATP site, namely, the "*DFG-in*" (type I) and "*DFG-out*" (type II) conformation. In order to address the question to which PDGF-Rβ-conformation compound **2** is likely to bind, we compared the molecular structure of **2** to a VEGF-R2-*DFG-in*-ligand (type I inhibitor pyridinyl-triazine, pdb 2p2h[10]) and to a prototypical *DFG-out* binder (type II inhibitor imatinib, pdb 2hyy[11]), respectively (Figure 1).

The binding pose overlay of the inhibitor structures in Figure 1 (shown as bound to the ATP binding pocket) suggests that compound **2** represents most likely a *DFG-in* binder. First, compared to the VEGF-R2-type-I pyridinyl-triazine inhibitor, compound **2** is matching well in terms of molecular shape. Furthermore, docked compound **2** is also occupying a

dx.doi.org/10.1021/jm500373x | J. Med. Chem. XXXX, XXX, XXX−XXX

Chart 2. Chemical Structures of the Potent 3,4-Diaryl-2*H*-pyrrole-2-one VEGF-R2/3 Inhibitor 1 and 3,5-Diaryl-pyrazin-2(1*H*)-one 2 of This Study Showing Comparable Decoration Patterns of the Aryl Moieties

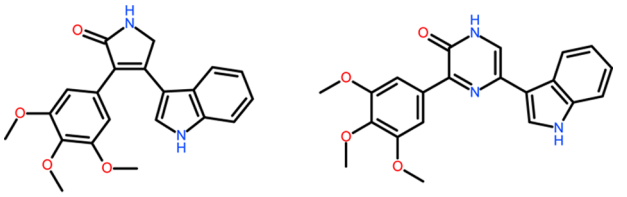

(1) (2)

Scheme 1. General Preparation Scheme of 3,5-Diaryl-pyrazin-2(1*H*)-ones (VI)[a]

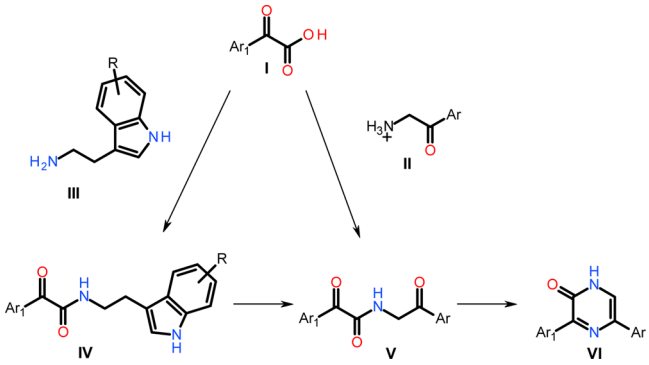

[a]The ketoamides (V) were prepared in two different routes, either via CDI mediated coupling of arylglyoxylic acid (I) and α-ketoamines (II) or via CDI mediated coupling of arylglyoxylic acid (I) and indolethylamines (III) to produce 2-oxo-2-phenyl-acetamides (IV), which yielded the corresponding (V) upon DDQ-oxidation. Final compounds (VI) were prepared in a microwave reaction using ammonium acetate as nitrogen source (method d). For clarity, the test compounds were numbered consecutively (**2**–**39**). Analytical data for all relevant compounds is available in Supporting Information.

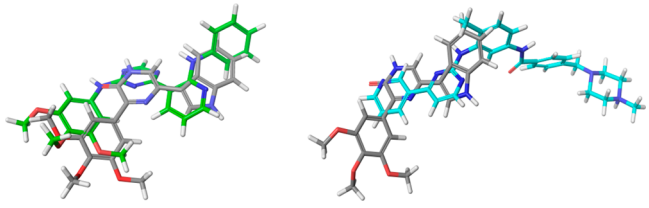

Figure 1. Left: Overlay of modeled docking pose of **2** (gray color) as oriented in the ATP binding pocket of VEGF-R2 and crystallographically determined binding mode of *DFG-in*/type I VEGF-R2 inhibitor 4-(2-anilinopyridin-3-yl)-*N*-(3,4,5-trimethoxyphenyl)-1,3,5-triazin-2-amine (green color, pdb 2p2h). Right: Superposition of docking pose of **2** (gray color) and *DFG-out*/type II inhibitor imatinib (light blue color, pdb 2hyy).

comparable space in the VEGF-R2 binding pocket. Second, the deep pocket binding part of the well-established *DFG-out*/type II-binder imatinib, namely, the 4-[(4-methylpiperazin-1-yl)-methyl]benzamide moiety, is not present in **2** (Figure 1, right). Third, docking of compound **2** into PK structures related to PDGF-Rβ possessing *DFG-out* conformations (Abl-kinase, pdb 2hyy;[11] VEGF-R2, pdb 3vhk[9] and 1t46;[12] c-src pdb, 3f3w[13]) revealed predicted binding poses in the ATP site not consistent with the originally present type II inhibitors. In contrast, plausible *DFG-in* binding modes were successfully calculated by docking experiments with **2** modeled in several *DFG-in* ATP-binding pockets (not shown) possessing significant sequence similarity to PDGF-Rβ (VEGF-R2, pdb 2p2h,[10] 3cjg,[14] and 3c7q;[15] fms, pdb 3lcd[16]). Therefore, on the basis of the highly related RTK VEGF-R2 we generated two PDGF-Rβ homology models, namely, using VEGF-R2 template structures in the *DFG-in* (pdb 2p2h[10]) and *DFG-out* conformation (pdb 1t46[12]), respectively. However, because only the *DFG-in* homology model proved to predict reasonable binding poses for **2** in the ATP binding pocket, this structure was used for further modeling studies in this project (Figure 2, pdb 2p2h; Schrödinger Prime,[17] version 3.2, Schrödinger, LLC, New York, NY, USA, 2013).

In order to validate the modeled hinge-binding mode of **2** in the ATP site of our PDGF-Rβ *DFG-in* homology model (Figure 2), we first synthesized and evaluated compounds **3** and **4** for their potency against PDGF-Rβ (Chart 3). Accordingly to our docking results the introduction of the 6-methyl group at the 3,5-diaryl-pyrazin-2(1*H*)-one core (compound **3**) is blocking the inhibitor's dual H-bond interactions to the hinge region (Glu101/Cys103) and thus killing the biological activity of **3**.

Likewise, compared to compound **2**, the lactam-regioisomeric structure **4** should be able to address an H-bond only to Glu101 but not be able to accept the H-bond from Cys103 thus showing reduced biological activity. In fact, the biological activities of **3** and **4** are in line with the proposed binding mode demonstrating a valid modeled pose of **2** in the active site of PDGF-Rβ. Motivated by the *in vitro* confirmation of our *DFG-in* homology model based binding mode, we retained the 3,5-diaryl-pyrazin-2(1*H*)-one core and next focused on the 3-aryl moiety.

Optimization of the 3-Aryl Substitution Pattern. According to the calculated binding mode the 3-aryl part of **2** is situated in the HRII which opens to the solvent (Figure 2). To further investigate the structure–activity relationships (SARs) and to optimize the 3-aryl system we used a straightforward docking/scoring approach. Although no direct ligand–protein interactions are involved in this area, our molecular docking campaign showed slight differences in the predicted binding affinities for variations of the methoxy-aryl substitution. As a result, compound **2** was top-ranked followed by **5**, **15**, and **7** (series 1, Table 1). For compounds **8** and **9** bearing an *ortho*-methoxy substitution (causing a 1*H*-pyrazin-2-one/3-aryl dihedral angle of almost 90°), no binding mode was predicted in the narrow ATP pocket. Further 3-aryl variations of **2** showed no significant docking scores. Hence, derived from the modeling approach we synthesized a selection of compounds (**5**–**15** showing systematic variations of the 1*H*-pyrazin-2-one-3-aryl moiety, series 1, Table 1), which were subsequently tested against PDGF-Rβ. Actually the docking/scoring results were reflected by the *in vitro* testing data. In accordance with the data of this series the 3-(3,4,5-trimethoxyphenyl) moiety in **2** was determined to be optimal: decreasing the number of methoxy groups (**5** and **6**) as well as positional changes of the aryl-methoxy groups (**7**, **8**, and **9**) resulted in diminished ligand affinity. Also, compared to hit compound **2**, the biological activity in this series could not be increased by introducing other moieties into the 3-aryl system such as morpholine (**12**), 4-fluor (**13**), 4-ethyl, or indole (**15**).

Optimization of the 5-Aryl Substitution Pattern. Therefore, we retained the 3-(3,4,5-trimethoxyphenyl)-1*H*-

dx.doi.org/10.1021/jm500373x | J. Med. Chem. XXXX, XXX, XXX–XXX

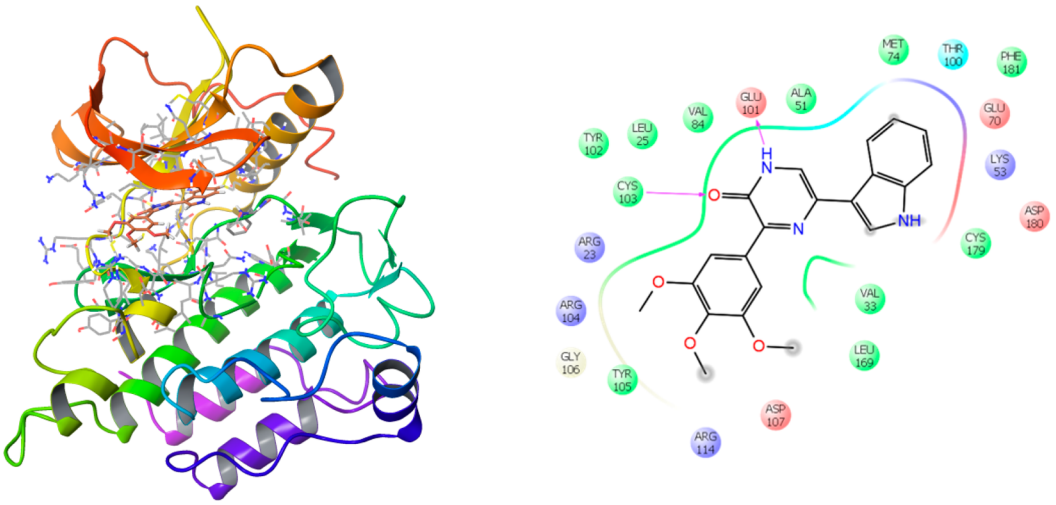

Figure 2. Left: *DFG-in* homology model of the PDGF-Rβ kinase domain based on the template structure of crystallographically determined VEGF-R2 (pdb 2p2h) and modeled binding mode of hit compound **2** (brown color) in the ATP binding pocket. Right: Ligand interaction diagram of modeled binding mode of **2** in the ATP binding pocket of the PDGF-Rβ PK domain. Key amino acid residues and ligand-active site interactions are shown. The central pyrazin-2(1*H*)-one core is involved in a dual H-bond interaction to the hinge region residues Glu101 and Cys103. The pyrazin-2(1*H*)-one 3-(3,4,5-trimethoxy) part is situated in the hydrophobic region II (HRII), whereas the pyrazin-2(1*H*)-one-5-(indole-3yl) part is occupying the hydrophobic pocket I (HPI).

Chart 3. Chemical Structures and Biological Activity against PDGF-Rβ (*in Vitro* Kinase Assay) of Key 3,5-Diaryl-pyrazin-2(1*H*)-ones 2, 3, and 4 to Confirm the Calculated Hinge-Binding Motif of 2 in the Homology-Modeled ATP Binding Pocket of the PDGF-Rβ PK

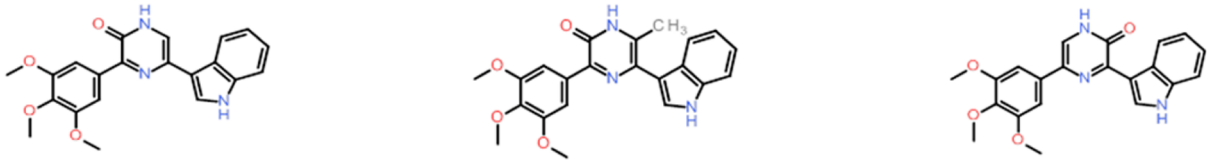

(**2**) PDGF-Rβ IC_{50} = 0.5 μM (**3**) PDGF-Rβ IC_{50} > 100 μM (**4**) PDGF-Rβ IC_{50} = 12 μM

Table 1. Series 1: SAR Data of Variations of Hit Compound 2 (PDGF-Rβ IC_{50} = 0.5 μM) Regarding the Pyrazin-2(1*H*)-one-3-aryl Substitution Pattern; Biological Activity Was Determined for Each Compound against PDGF-Rβ in an *in Vitro* Kinase Assay

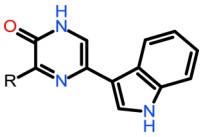

#	R	PDGF-Rβ IC_{50} [μM]	#	R	PDGF-Rβ IC_{50} [μM]
2		0.5	**10**		5
5		1.5	**11**		13
6		19	**12**		13
7		4	**13**		12
8		> 100	**14**		32
9		> 100	**15**		2

pyrazin-2-one system, and for further optimization of **2** we next concentrated on variations of the 5-indole moiety, which is situated in the buried HPI (Figure 2). We first generated a focused virtual set of substituted 5-indole variations of compound **2** and performed docking experiments using the PDGF-Rβ homology model structure (Schrödinger GlideSP,[18] version 5.9, Schrödinger, LLC, New York, NY, USA, 2013). From the top-ranked docking hits (Figure 3) we prepared 14 synthetically accessible compounds and tested those for their biological activity against PDGF-Rβ (series 2, Table 2).

In line with the calculated modeling data compounds, **16**, **24**, and **27** were indeed determined to show good activity against PDGF-Rβ (Table 2). The naphtyl moiety of **24** (IC_{50} PDGF-Rβ = 1 μM) is filling the HPI, whereas the 5′-hydroxyindole in **16** (IC_{50} PDGF-Rβ = 0.3 μM) is addressing an additional H-bond to the gatekeeper residue Thr100 (Figure 3). Only the biological activity against PDGF-Rβ of compound **16** (showing the 5′-hydroxyindole decoration) was determined to be in the sub-μM range (as was the parent compound **2**). However, the flat *in vitro* SARs for further compounds of this 1*H*-pyrazin-2-one-5-aryl series 2 (**17**−**29**, see Table 2) poorly matches the docking/scoring of the compounds. In contrast to the good correlation of predicted ligand−protein interactions of our PDGF-Rβ homology model with the SAR (series 1), so far these results may indicate a structural misarrangement regarding the HPI in our model. However, the inconsistency

dx.doi.org/10.1021/jm500373x | *J. Med. Chem.* XXXX, XXX, XXX−XXX

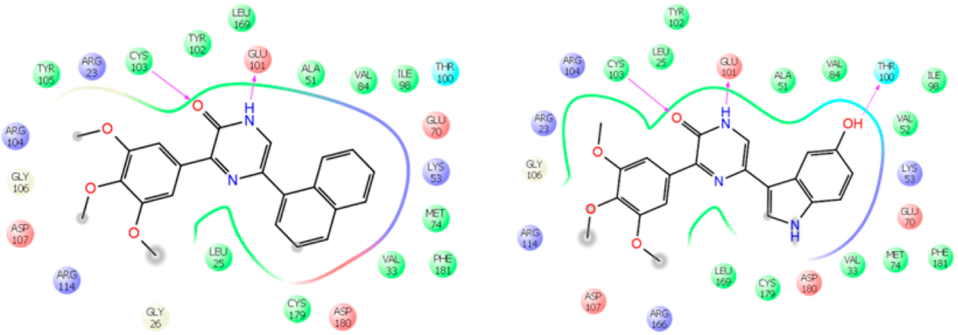

Figure 3. Ligand interaction diagram of top-ranked compounds **24** (left) and **16** (right) in the ATP binding site of the PDGF-Rβ homology model. Key amino acid residues and ligand–active site interactions are shown. GlideSP ranking of the compounds (top-down): **24**, **16**, **27**, **29**, **18**, **28**, **22**, **21**, **20**, **19**, **2**, **17**, **16**, **25**, and **23**.

Table 2. Series 2: SAR Data of Variations of Hit Compound 2 (PDGF-Rβ IC_{50} = 0.5 μM) Regarding the Pyrazin-2(1*H*)-one-5-aryl Substitution Pattern

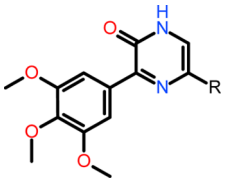

#	R	PDGF-Rβ IC_{50} [μM]	#	R	PDGF-Rβ IC_{50} [μM]
16		0.3	**23**		26
17		1	**24**		1
18		14	**25**		8
19		56	**26**		2
20		2	**27**		1
21		9	**28**		2
22		3	**29**		7

of the modeling/*in vitro* SAR correlation for this pocket could refer to particular parameters triggering ligand affinity, which are not sufficiently implemented in the applied docking/scoring process.

WaterMap Calculations. Namely, this phenomen may be explained by the thermodynamic contribution of displacing water molecules, predominantly in hydrophobic binding pockets. It is considered to be a key factor for ligand affinity ("hydrophobic effect").[19] In order to investigate if entropic critically water molecules in the ATP binding pocket of PDGF-Rβ could be predictable parameters for the optimization of 3,5-diaryl-pyrazin-2(1*H*)-ones in our project, we calculated hydration sites in the PDGF-Rβ homology model apo-structure by using the WaterMap technology[17,18] (Figure 4). The WaterMap method combines calculations for molecular dynamics, solvent clustering, and statistical thermodynamics to assess the enthalpy, entropy, and free energy of water "hydration sites". Moreover, WaterMap has been successfully applied to study parameters driving selectivity for ligands in the ATP pocket of protein kinases.[20] Having the WaterMap results for the PDGF-Rβ homology model apo structure in hand, we designed a set of 5-phenyl variations of the 3-(3,4,5-trimethoxyphenyl)-1*H*-pyrazin-2-one scaffold (compounds **30**–**38**, series 3, Table 3). Herein, the concept of the 5-phenyl decoration was based on the idea to investigate SARs in terms of the displacement of hydration sites. In turn, all compounds of this project were docked into the ATP pocket of our PDGF-Rβ homology model. As an outcome, compound **38** was calculated to be the top hit of this docking campaign. Strikingly, the predicted high affinity of **38** was confirmed by the *in vitro* assay (**38** IC_{50} PDGF-Rβ = 0.02 μM, Table 3) demonstrating this compound to be the most potent inhibitor of all three series. The docking pose actually shows that the majority of key hydration sites calculated by WaterMap were displaced by the inhibitor (Figure 4). In detail, the 3-(3,4,5-trimethoxyphenyl) moiety displaces all relevant hydration sites in the HRII. In the hinge region two of the most unstable hydration sites (colored in red) are displaced by the lactam moiety of the 1*H*-pyrazin-2-one core. This approach also offers a strong structural explanation for the comparable high affinity of this lactam-regioisomer (also see **2** versus **4**, Chart 3). Most notably, within the HPI the 4′-phenolic OH of **38** is not only displacing an unstable hydration site (colored in light red) but this OH group is also replacing a stable water molecule (colored in green), positioning the OH function in an H-bond network between Lys53 and Asp180 (Figure 4). This water replacement should be unfavorable in terms of entropy but can be compensated by enthalpy summing up to a total decrease of Gibbs free energy (ΔG). In addition, the vicinal 3′-methoxy group of **38** displaces two unstable hydration sites in the rear HPI. However, two hydration sites imbedded by Val33, Val84, Ile98, and Met74 were not yet affected by the present inhibitors. Hence, the displacement of these water molecules will be the subject of our ongoing inhibitor optimization strategy.

Considering the displacement of hydration sites (Figures 4 and 5; for complete data, see Supporting Information), a differentiated analysis regarding the contribution of various functional groups at the phenyl moiety toward ligand affinity can be discussed[21] based on the SAR data of series 3 (Table 3). The phenolic-4′-OH is essential for potent ligand affinity toward PDGF-Rβ as compounds **35** and **38** show IC_{50}values in the sub-μM range. In contrast, compounds having 4′-methoxy (**30** and **37**) or 4′-chloro (**32**) substitutions were determined to be significantly less active. Interestingly, the phenyl-3′-substituted compounds **31** (3-methoxy, IC_{50} PDGF-Rβ = 1.4 μM) and **33** (3-chloro, IC_{50} PDGF-Rβ = 0.8 μM) are moderate binders. This may be due to displacement of the two hydration sites #8 and #83 with unfavorable ΔG (see Figure 5 and Supporting Information) at the rear pocket while leaving the

dx.doi.org/10.1021/jm500373x | *J. Med. Chem.* XXXX, XXX, XXX–XXX

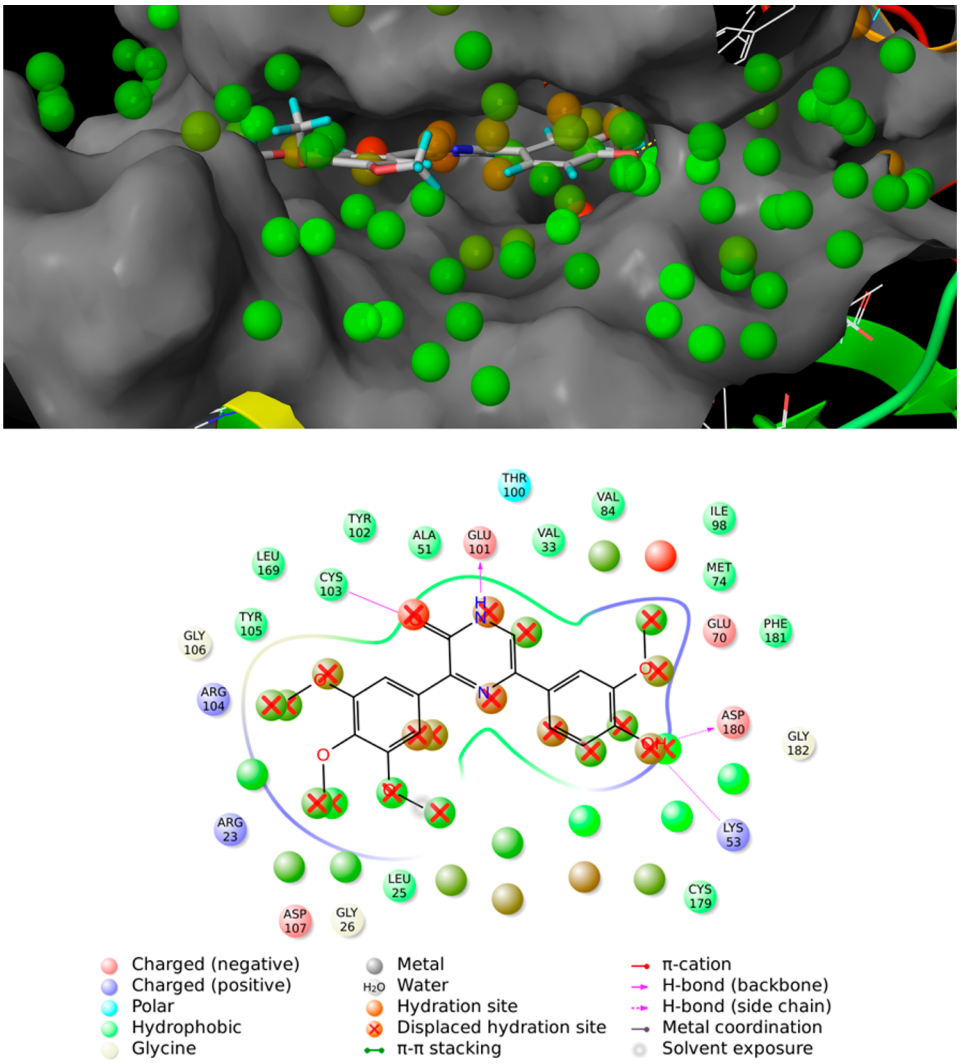

Figure 4. Top: Docking pose of **38** (PDGF-Rβ IC_{50} = 0.02 μM) in the ATP binding pocket of the PDGF-Rβ PK homology model domain showing the molecular surface (docking by Glide) and overlay of hydration sites (colored spheres; for color code, see below) calculated by WaterMap. Bottom: Ligand−protein interaction diagram of **38** in the ATP binding pocket of the PDGF-Rβ homology model. Key hydration sites from WaterMap calculations on the PDGF-Rβ homology model apo-structure are superimposed to illustrate the displacement of hydration sites by the inhibitor. Hydration sites shown as red spheres represent "unstable" water molecules. Their displacement results in an increase of environmental entropy ("hydrophobic effect"). Green spheres symbolize "stable" water molecules, which should not be displaced by an inhibitor in terms of unfavorable enthalpic effects.

structural water #13 between Lys53 and Asp180 in place (with favorable ΔG). The phenyl-2′-substituted compounds **34** (2-chloro, IC_{50} PDGF-Rβ = 5 μM) and **36** (phenolic-2-OH, IC_{50} PDGF-Rβ = 2 μM) also showing moderate affinity indicate sterical space at this part of the binding site (hydration site #34). Thus, the 2′-phenyl position of this series may be suitable for further ligand optimization regarding interactions to the HPI.

On the basis of the PDGF-Rβ IC_{50} values of compounds **31**, **35**, **38**, and **39**, we quantified the relative contribution of the 3′-methoxy and the 4′-hydroxyphenyl substituents toward the experimental ΔG of these inhibitors. The values of ΔG are based on the calculation[21] of $\Delta G = -RT \cdot \ln IC_{50}$, Figure 5). Within this set of compounds the 4′-hydroxy moiety contributes approximately −11 kJ/mol to the actual free binding enthalpy, while the 3′-methoxy moiety (∼−4.3 kJ/mol) adds 3-fold less value to ΔG. In this regard, the WaterMap calculations are in good accordance: the 4′-hydroxy moiety is replacing the hydration site #13 for which an entropic term of 15.5 kJ/mol has been calculated. The 3′-methoxy moiety is displacing hydration site #83 with a calculated $-T\Delta S$ of 4.8 kJ/mol (indicating the methoxy-oxygen to partly compensates the hydration site oxygen). In addition to the SAR discussed above, these numbers further highlight the importance of the phenyl 4′-hydroxy moiety in terms of replacing a structural water molecule.

The most potent PDGF-Rβ-inhibitors of the 1*H*-pyrazin-2-ones were tested against the closely related PK VEGF-R2 and c-kit (Table 4). Herein, compound **38** showed only moderate 10-fold selectivity for PDGF-Rβ over VEGF-R2 and c-kit suggesting comparable *DFG-in* binding modes in these kinases, which is in line with the findings of Furet et al.[22] In their study it is shown that PK having a cysteine residue in the *DFG*-minus-1-position favor *DFG-in* binding of ligands that can form a sulfur−aromatic interaction to this cysteine. In fact, in the binding mode of the ligands in our PDGF-Rβ model this is the case for Cys179 (D180-F181-G182, also see LID Figure 2, right, and Figure 4, bottom) explaining why in addition to

dx.doi.org/10.1021/jm500373x | J. Med. Chem. XXXX, XXX, XXX−XXX

Table 3. Series 3: SAR Data of Variations of Hit Compound 2 (PDGF-Rβ IC_{50} = 0.5 μM) Regarding the Pyrazin-2(1*H*)-one-5-phenyl Substitution Pattern[a]

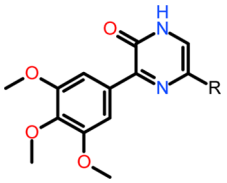

#	R	PDGF-Rβ IC_{50} [μM]	#	R	PDGF-Rβ IC_{50} [μM]
30		22	**35**		0.1
31		1.4	**36**		2
32		31	**37**		19
33		0.8	**38**		0.02
34		5	**39**		8

[a]The design of the phenyl decoration was based on joined WaterMap/Glide docking calculations. The biological activity against PDGF-Rβ of compound **38** (PDGF-Rβ IC_{50} = 0.02 μM) showing the phenyl-3′-methoxy-4′-hydroxy decoration could be significantly improved compared to the parent hit compound **2**.

PDGF-Rβ these compounds also potently inhibit VEGF-R2 and c-kit (and Flt3, see Table 4 and Figure 6).

Table 4. Biological Activity of Selected Compounds against PDGF-Rβ and the Closely Related PK VEGF-R2 and c-kit (Activated Kinase Assays, for Details See Experimental Section)

	PDGF-Rβ	VEGF-R2	c-kit
#	IC_{50} (μM)	IC_{50} (μM)	IC_{50} (μM)
2	0.5	2.3	0.9
16	0.3	1.0	2.7
31	1.4	23	7.4
33	0.8	56	2.4
35	0.1	2.2	0.4
38	0.02	0.2	0.2

Furthermore, compound **38** was profiled for selectivity at a concentration of 1 μM in a panel of 300 wild-type kinases. Herein, **38** most potently inhibited PDGF-Rβ (residual activity = 1%) but also blocked further PKs, albeit to a lesser extent (Figure 6, also see Supporting Information). However, compound **38** could be shown to be a promising hit with reasonable selectivity for further optimization toward an effective PDGF-Rβ inhibitor for clinical use.

Cellular Assays. Furthermore, we evaluated a selection of potent inhibitors of this project for their cytotoxic profiles using five different cell lines including HL-60, a human myeloblastic leukemia cell line (Figure 7). It has been shown that the proliferation and differentiation particularly of the HL-60 cells depend upon PDGF-R signaling.[23] Cells were treated with the

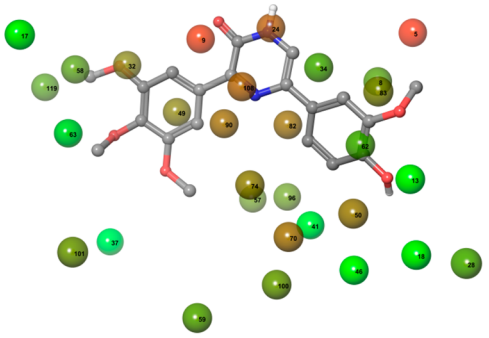

Hydration site #	ΔH	-TΔS	ΔG
13	-31.4	15.5	-15.9
83	5.1	4.8	9.9

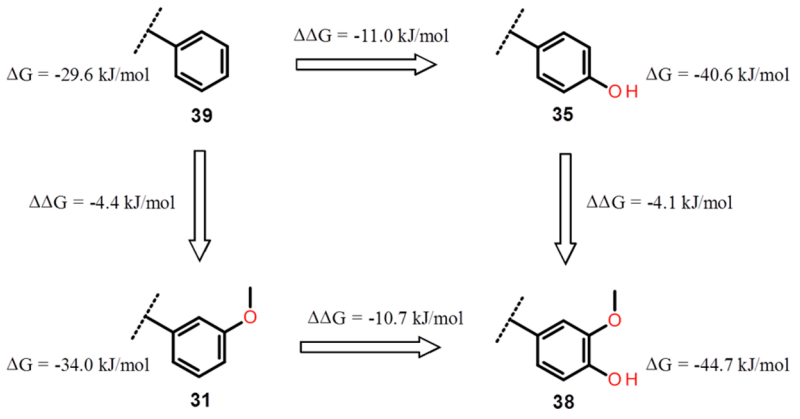

Figure 5. Top: Overlay of **38** (only polar hydrogens shown) and selected WaterMap hydration sites (within 5 Å of the ligand and ΔG > 4.2 kJ/mol or < −4.2 kJ/mol) in the PDGF-Rβ homology model apo-structure. The hydration sites are numbered consecutively and are colored based on their respective ΔG values in kJ/mol from red/unstable to green/stable. For the key hydration sites #13 and #83, calculated ΔG, enthalpies, and entropies (in kJ/mol) with respect to bulk solvent are shown (complete data for all hydration sites can be found in the Supporting Information). Below: Experimentally determined relative contribution of 3′-methoxy and 4′-hydroxy phenyl-substituents to ΔG of the inhibitors **31** (IC_{50} = 1.4 μM), **35** (IC_{50} = 0.1 μM), **38** (IC_{50} = 0.02 μM), and **39** (IC_{50} = 8 μM) against PDGF-Rβ.

dx.doi.org/10.1021/jm500373x | J. Med. Chem. XXXX, XXX, XXX−XXX

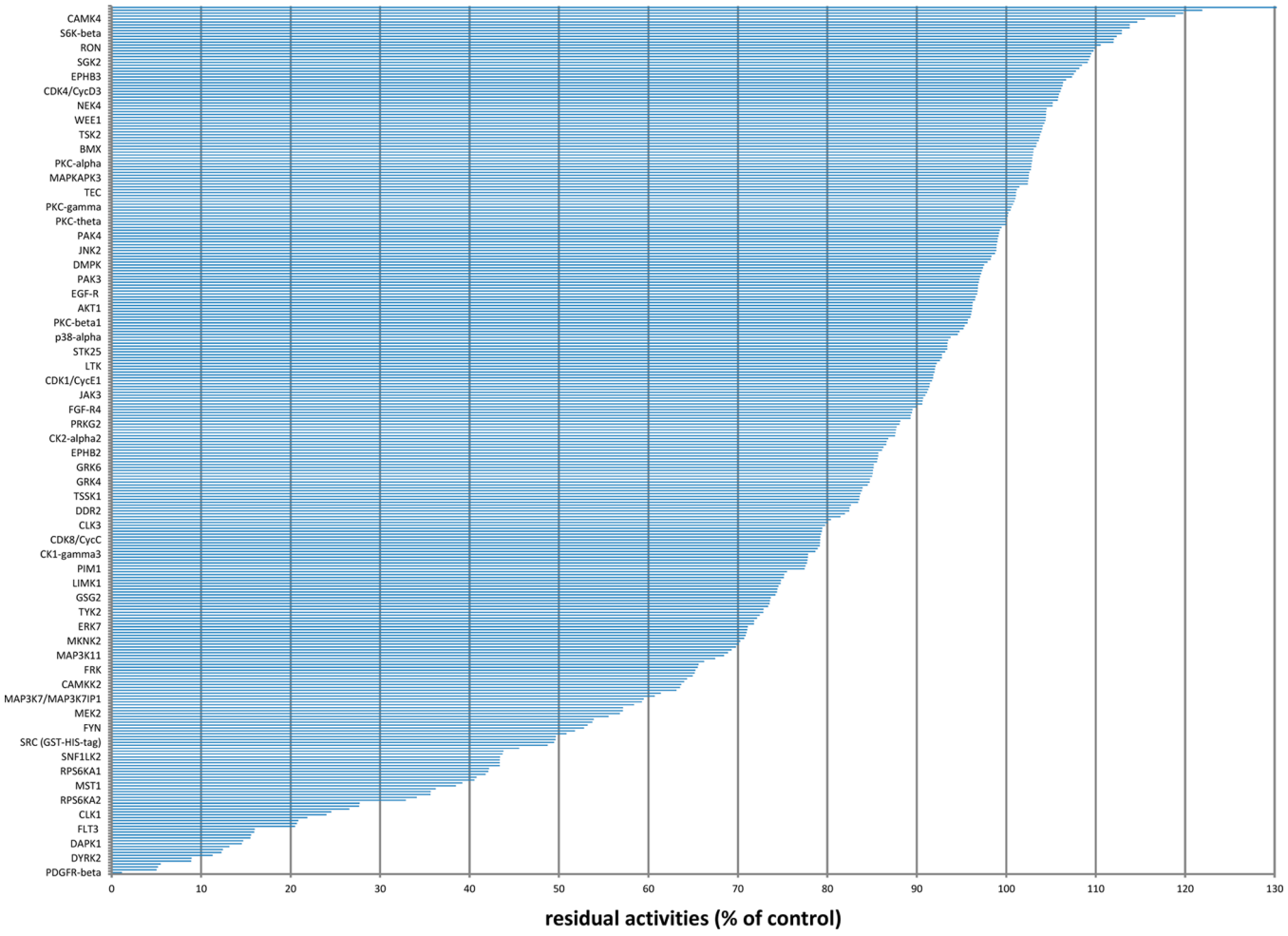

Figure 6. Graphical representation of the selectivity profile of compound **38** at a concentration of 1 μM against 300 wild-type protein kinases (mean of duplicate measurements). For clarity of representation, not all PK are shown at the *y*-axis (for full details see Supporting Information). PKs showing residual activity less than 50%: PDGF-Rβ (1%), RET (5%), HIPK4 (5%), CLK4 (5%), RIPK2 (9%), DYRK2 (9%), ACV-R2B (11%), LRRK2 (12%), CLK2 (12%), ACV-R1 (13%), DAPK1 (15%), MELK (15%), RPS6KA6 (16%), ACV-RL1 (16%), DYRK1B (16%), FLT3 (16%), DYRK3 (20%), VEGF-R2 (21%), DAPK3 (21%), PIM3 (22%), CLK1 (24%), DAPK2 (25%), RPS6KA3 (27%), CSF1-R (28%), TGFB-R2 (28%), RPS6KA2 (33%), HIPK2 (34%), TRK-C (36%), MST2 (36%), FGR (36%), MST1 (38%), FGF-R2 (39%), ARK5 (41%), VEGF-R3 (41%), KIT (42%), RPS6KA1 (42%), HIPK1 (42%), BLK (43%), DYRK1A (43%), IRAK4 (43%, SNF1LK2 (43%), TRK-A (44%), MERTK (44%), ITK (46%), CDK5/p35NCK (49%), SRC (49%), DYRK4 (50%), and TRK-B (50%). For assay details and abbreviations also visit www.proqinase.com.

test compounds and their viability was determined after 48 h incubation. All test compounds were shown to be cytotoxic against HL-60 cells. Interestingly, the other cells tested were significantly less affected by treatment of **2**, which is in line with the notion that HL-60 cells depend on PDGF-R signaling. Compound **2** was determined to have an IC_{50} value of 0.026 μM against HL-60 cells[1] and exhibited a significantly stronger antiproliferative effect than **38** that had an IC_{50} value of 3.2 μM in this assay. However, even if **38** showed to be most potent against HL-60 cells within the other cell lines tested in this project, the reduced cellular efficacy of **38** compared to **2** is in sharp contrast to the data from isolated PDGF-Rβ assay (Table 4). This may be due to inferior ADME properties such as limited cellular bioavailability, unspecific protein binding, or a metabolic inactivation particularly of the key phenolic−OH moiety of **38**. Thus, in order to estimate the cellular uptake of **38**, an assay was performed using Caco-2 cells[25] (Figure 8).

The data shows that compound **38** is slowly penetrating into the cells reaching a maximum intracellular concentration of approximately 40% after 60 min of incubation time. The cellular uptake is paralleled by a decrease of **38** in the assay medium. However, although this data provides evidence for a moderate cellular bioavailability of **38**, the total recovery of the inhibitor (in both portions, medium and intracellular) was determined to be approximately 70%. As discussed above this may be due to unfavorable ADME properties of **38** such as nonspecific protein binding and metabolization.

Effect of Compound 38 on the Signal Transduction in U87 Cells. In order to analyze the effect of **38** on the PDGF signal transduction, a Western blot experiment was performed using U87 cells. Herein, the phosphorylation of Akt and ERK upon PDGF BB stimulation in the absence and presence of **38** was determined in a concentration-dependent manner (Figure 9). In this experiment **38** was able to decrease significantly the phosphorylation of AKT at a concentration of 3 μM. Furthermore, the ERK phosphorylation was less affected as expected for an inhibitor blocking PDGF-R signaling.[26]

dx.doi.org/10.1021/jm500373x | J. Med. Chem. XXXX, XXX, XXX−XXX

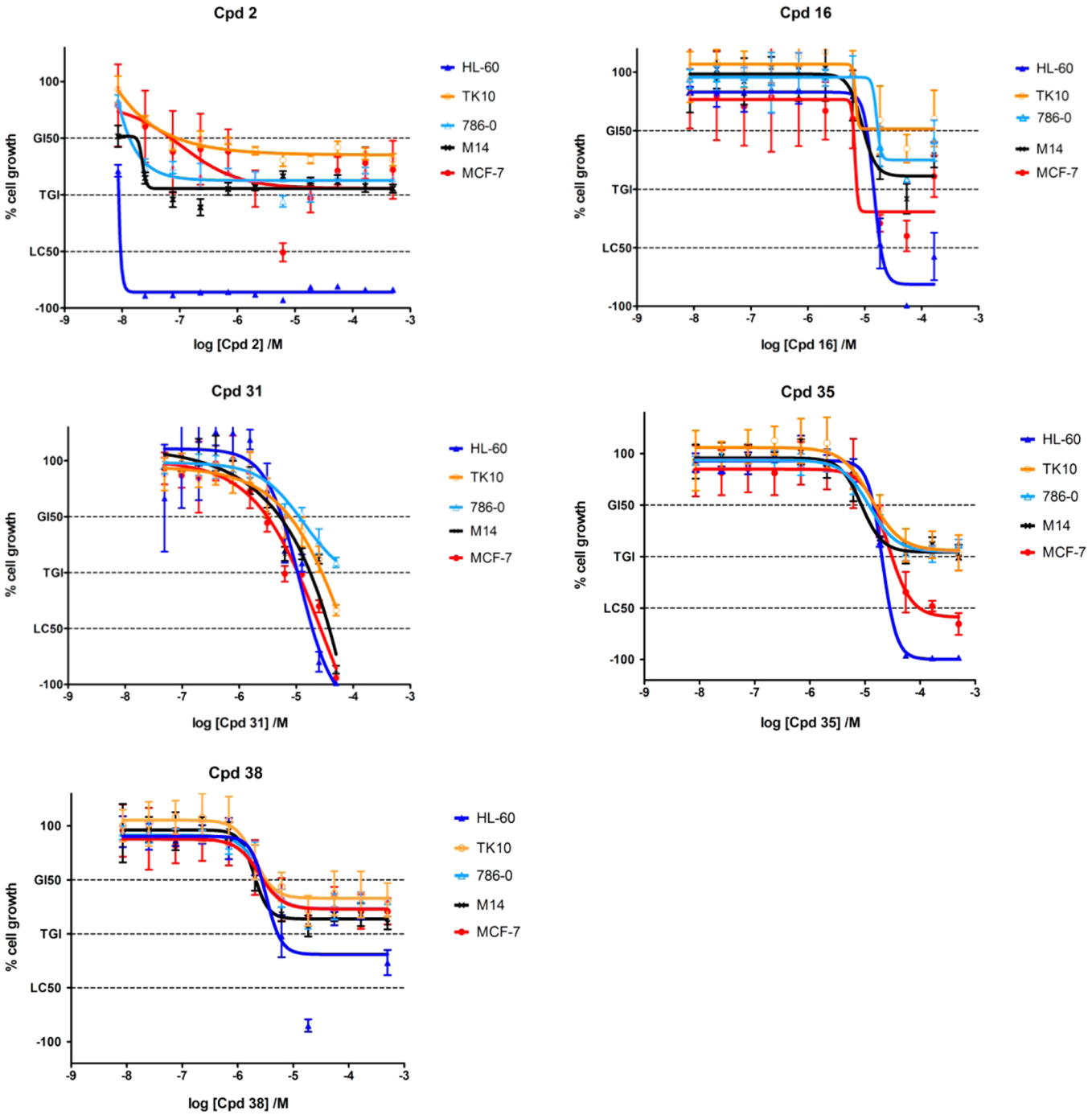

Figure 7. Determination of cytotoxic profiles of compounds **2**, **16**, **31**, **35**, and **38** in cell viability assays using HL-60, TK 10, 786-0, M14, and MCF-7 cell lines.

CONCLUSIONS

In this article we demonstrate the successful optimization of 3,5-diaryl-pyrazin-2(1*H*)-ones as potent PDGF-Rβ inhibitors. SARs for three pyrazin-2(1*H*)-ones series showing variable 3,5-aryl substitution patterns have been investigated. The 3,4,5-trimethoxy system at the 3-aryl position proved to be optimal and was therefore retained for further optimization. This moiety is situated in the HRII where the molecular modeling correlated accurately with the biological data. However, standard docking/scoring only insufficiently reflected the impact of the "hydrophobic effect" in the HPI where the 5-aryl system is located. The thermodynamic contribution of displacing water molecules from key hydration sites could be calculated by the WaterMap technology. This approach led to the design of compounds featuring both displacement and replacement of key hydration sites. Herein, the gain in ligand affinity can be explained by the displacement of key hydration sites of the 3,5-diaryl-pyrazin-2(1*H*)-one core scaffold. Moreover, the replacement of a structural water molecule in the active site by the 4′-phenolic OH group of **38** in combination with the displacement of two further unstable hydration sites by the vicinal 3′-methoxy moiety of **38** essentially contributes to the ligand's affinity. This resulted in a 25-fold increase of the IC_{50} value for **38** (PDGF-Rβ: IC_{50} = 0.02 μM) compared to the

dx.doi.org/10.1021/jm500373x | *J. Med. Chem.* XXXX, XXX, XXX−XXX

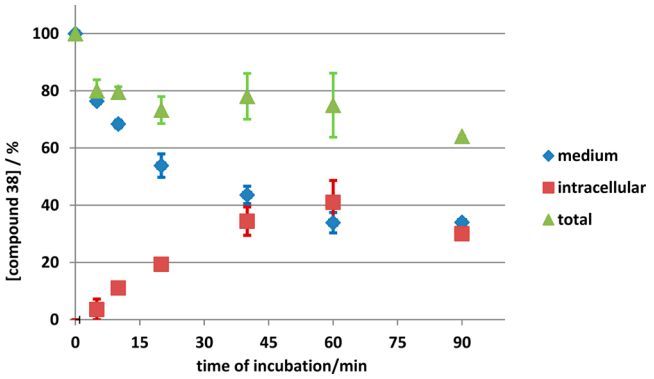

Figure 8. Measurement of the cellular uptake of **38** using a Caco-2 model. Cells were incubated with **38** at a concentration of 50 μM for 90 min, and the amount of **38** in the medium as well as the intracellular portion of **38** was determined by HPLC analysis (a control experiment using propranolol was performed; for further details see Supporting Information).

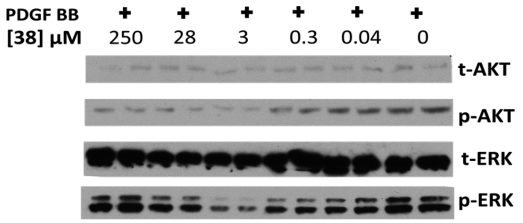

Figure 9. Effect of **38** on the signaling in U87 cells. The cells were treated with the indicated concentrations of **38** for 60 min at 37 °C and stimulated with 10 ng/mL PDGF BB for 10 min. Cells were lysed and lysates immunoblotted with the indicated antibodies (for details see Supporting Information). Similar results were obtained in duplicate experiments.

hit compound **2** (PDGF-Rβ: IC_{50} = 0.5 μM). A selectivity profile in a panel of 300 PKs was determined for **38** showing the compound to most potently block PDGF-Rβ activity. However, the promising activity of **38** in the kinase assay did not fully translate into potent efficacy in cellular assays as analyzed by Western blot. The moderate cellular efficacy of **38** may be due to the compound's limited ADME properties such as inferior cellular bioavailability based on poor permeability or the susceptibility to metabolic degradation particularly of the phenolic hydroxy moiety. Further hit-to-lead development of this compound series toward potent PDGF-Rβ inhibitors is therefore essential.

EXPERIMENTAL SECTION

^{1}H (300 MHz) and ^{13}C (75 MHz) NMR were recorded on a Bruker Avance III 300 spectrometer (Rheinstetten, Germany) at 300 K with a multinuclear probe head using the manufacturer's pulse programs. The data are reported as follows: chemical shifts in ppm from Me_4Si (TMS) as external standard, multiplicity, and coupling constant (Hz). NMR spectra were obtained, and ^{1}H (300 MHz) and ^{13}C spectra (75 MHz) were referenced either to TMS or to internal DMSO-d_5 (^{1}H NMR δ 2.50) and internal DMSO-d_6 (^{13}C NMR δ 39.5) or internal $CHCl_3$ (^{1}H NMR δ 7.26) and internal $CDCl_3$ (^{13}C NMR δ 77.0). All coupling constants (J values) are quoted in Hz. The following NMR abbreviations are used: b (broad), s (singlet), d (doublet), t (triplet), and m (unresolved multiplet). The labeling scheme of structures to correlate NMR signals can be found in Supporting Information.

Mass spectra of the compounds were recorded after chromatographic separation. Mixtures were separated with an Agilent 1100 HPLC system (Waldbronn, Germany) consisting of a thermostated autosampler, diode array detection, and an Agilent Zorbax Eclipse XDB-C8 column (150 × 4.6 mm, 5 μm particle size). Elution was achieved with a solvent gradient system of water and acetonitrile, with 0.1% of acetic acid and a flow rate of 1 mL/min. The eluent flow was splitted to the mass spectrometer.

Mass spectra with nominal resolution were recorded with an Esquire ~LC mass spectrometer (Bruker Daltonik, Bremen, Germany), with electrospray ionization operating in the positive ion mode, with the following parameters: drying gas nitrogen 8 l/min, nebulizer 35 psi, dry gas heating 350 °C, HV capillary 4000 V, and HV end plate offset −500 V. GC/MS was performed on a HP6890 Series System. EI-mass spectra were recorded on a Varian MAT 311A (70 eV). HRMS spectra were recorded on a MAT-95 (Finnigan).

Where appropriate, column chromatography was performed for crude precursors with Merck silica gel 60 (0.063−0.200 mm) or Acros organics silica gel (0.060−0.200 mm; pore diameter ca. 60 nm). Column chromatography for test compounds was performed using a LaFlash system (VWR) with Merck silica gel 60 (0.015−0.040 mm) or RP8 columns. The progress of the reactions was monitored by thin-layer chromatography (TLC) performed with Merck silica gel 60 F-245 plates. Where necessary, reactions were carried out in a nitrogen atmosphere using 4 Å molecular sieves. All reagents and solvents were obtained from commercial sources and used as received (THF was used after distillation over K/benzophenone). Reagents were purchased from Sigma-Aldrich Chemie, Steinheim, Germany; Lancaster Synthesis, Mühlheim, Germany; or Acros, Nidderau, Germany.

HPLC analysis was performed on a Hewlett-Packard HP 1090 Series II using a Thermo Betasil C8 (150 × 4.6 mm 5 μM) column (mobile phase flow 1.5 mL/min, gradient KH_2PO_4 buffer pH 2.3/methanol, UV-detection 230/254 nm). All key compounds submitted to biological assays were proven by this method to show ≥98% purity.

Synthesis of Compounds. Synthesis of arylglyoxylic acids (I, Scheme 1) was achieved by SeO_2-mediated oxidation of the respective acetophenone in pyridine.[24] The α-ketoamines (II, Scheme 1) were prepared either by Delépine reaction from acetophenones[27] or by using aryl acids as starting material.[28] The open-chained diketoamides (V, Scheme 1) were synthesized via two different routes: (a) by CDI-mediated coupling of arylglyoxylic acids I and aryl α-ketoamines II or (b) by CDI-mediated coupling[7] of arylglyoxylic acids I and indole derivatives III to yield indole-amides IV. Subsequent DDQ oxidation[1] of the indole side-chain in IV yielded indole-diketoamides V. All test compounds were synthesized in the final step accordingly to the general microwave mediated method using ammonium acetate as nitrogen source:[1] a microwave vial (5 mL) was equipped with ammonium acetate (10 equiv) and a solution of open-chained diketoamide V (1 equiv) in 3 mL acetic acid (total volume). The vial was sealed and stirred at 160 °C for 4 min in a microwave synthesizer (CEM Discover). The reaction vessel was cooled to rt when H_2O was added to precipitate the raw pyrazinone, which was filtered off and purified by preparative HPLC (RP-phase) to afford the test compound in ≥98% purity.

The experimental procedures for the preparation of compounds **5**, **6**, **8**, **12**, **13**, **15**, and **31** are reported in our recent study.[7] The experimental procedure for the preparation of compounds **2** and **16** are reported in the literature.[1] The analytical data for the other compounds of this article (**3b**/**3c**/**3**, **4a**/**4**, **7b**/**7c**/**7**, **9b**/**9c**/**9**, **10b**/**10c**/**10**, **11b**/**11c**/**11**, **14b**/**14c**/**14**, **17b**/**17c**/**17**, **18a**/**18**, **19a**/**19**, **20b**/**20c**/**20**, **21a**/**21**, **22a**/**22**, **23a**/**23**, **24a**/**24**, **25a**/**25**, **26a**/**26**, **27a**/**27**, **28a**/**28**, **29a**/**29**, **30a**/**30**, **32a**/**32**, **33a**/**33**, **34a**/**34**, **35a**/**35**, **36a**/**36**, **37a**/**37**, **38a**/**38**, and **39a**/**39**) can be found in the Supporting Information. X-ray data for compounds **24** (CCDC number: 986158) and **29a** (CCDC number: 986159) is also given in the Supporting Information.

Molecular Modeling. All modeling was performed on a DELL 8 core system. For preparation, visualization and building the 3D structures Maestro (version 9.3) from Schrödinger (Schrödinger, LLC, New York, NY, 2013) was used. The illustrations of modeling were generated by Maestro. For compound docking and screening the Schrödinger "Glide SP" workflow was used.[18] The goal of the Glide

dx.doi.org/10.1021/jm500373x | J. Med. Chem. XXXX, XXX, XXX−XXX

methodology is to semiquantitatively rank the ability of candidate ligands to bind to a specified conformation of the protein receptor.[29] Prior to determining binding poses of ligands, energetically minimized compound conformations were generated, docked into the active site, and subsequently ranked based on their calculated binding affinity. The homology model for PDGF-Rβ was performed using the Prime workflow,[16,30] primary sequence data of PDGF-Rβ (http://www.uniprot.org/uniprot/P09619), and the VEGF-R2 template structures in the *DFG-in-* (pdb 2p2h) and *DFG-out*-conformation (pdb 1t46), respectively.

WaterMap computes water properties (location, occupancy, enthalpy, entropy, and free energy) through a combination of molecular dynamics, solvent clustering, and statistical thermodynamic analysis. First, a 2 ns explicit-solvent molecular dynamics simulation of the protein with the ligand removed is run in order to sample the configurations of water molecules in the binding site. The coordinates of the protein are restrained with a 5.0 kcal/mol/A^2 harmonic potential applied to the initial positions of the heavy atoms, which ensures convergence of the water sampling around the protein conformation of interest. Waters from approximately 2000 equally spaced frames from the molecular dynamics simulation are then spatially clustered to form localized hydration sites, and the thermodynamic properties of those sites are computed. The enthalpy is computed as the average nonbonded molecular mechanics interaction energies of the waters in the hydration site with the rest of the system. The entropy is computed by numerically integrating a local expansion of spatial and orientational correlation functions, as described in the inhomogeneous solvation theory work by Lazaridis.[31] The relevant solvation thermodynamic quantities for the ligand are computed based on the amount of overlap with the hydration sites.

Biological Evaluation. All inhibitor solutions were prepared freshly in DMSO prior to each experiment and used immediately.

Determination of IC_{50} Values of Compounds. *Recombinant Protein Kinases.* The inhibitory profile of compounds was determined using the following 24 protein kinases (GenBankAcc. No. available on http://www.proqinase.com/pages/science): AKT1, ARK5, Aurora-A, Aurora-B, B-Raf-VE, CDK2/CycA, CDK4/CycD1, CK2-A1, EGF-R, EPHB4, ERBB2, FAK, IGF1-R, SRC, VEGF-R2, VEGF-R3, FLT3, INS-R, MET, PDGF-Rβ, PLK1, SAK, TIE2, and COT. All protein kinases were expressed using human cDNAs in Sf9 insect cells as recombinat GST-fusion proteins or His-tagged proteins by means of the baculovirus expression system. Kinases were purified by affinity chromatography using either GSH-agarose (Sigma) or Ni-NTH-agarose (Qiagen). The purity and identity of each kinase was determined by SDS-PAGE/silver staining and Western blot analysis using specific antibodies.

Protein Kinase Assay. A proprietary protein kinase assay (^{33}PanQinase Activity Assay) was used for measuring the kinase activity of the 24 protein kinases. All protein kinase assays were performed in 96-well FlashPlatesTM (PerkinElmer/NEN, Boston, MA, USA) in 50 μL reaction volumes. Assays for all enzymes were performed in a solution containing 60 mM HEPES-NaOH, pH 7.5, 3 mM $MgCl_2$, 3 mM $MnCl_2$, 3 μM Na-orthovanadate, 1.2 mM DTT, 50 μg/mL PEG20000, 1 μM [γ-^{33}P]-ATP (approximately 5 × 10^5 cpm per well), and recombinant protein kinase (50−400 ng). Depending upon the kinase being assayed, appropriate substrates were used and were as follows (substrates shown in parentheses): AKT1 (GSK3/14−-27), ARK5 (autophosphorylation), Aurora-A, Aurora-B (Tetra-(LRRWSLG)), B-Raf-V600E (MEK1 KM), CDK2/CycA (histone H1), CDK4/CycD1 (Rb-CTF), CK2-A1 (casein), EGF-R, EPHB4, ERBB2, FAK, IGF1-R, SRC, VEGF-R2, VEGF-R3 (poly(Glu,Tyr) 4:1), FLT3, INS-R, MET, PDGF-Rβ (poly(Ala,Glu,Lys,Tyr) 6:2:5:1), PLK1 (casein), SAK (autophosphorylation), TIE2 (poly(Glu,Tyr) 4:1), and COT (autophosphorylation). The IC_{50} values were measured by testing 10 concentrations of compounds in singlicate. The final DMSO concentration in the assay was 1% (v/v). The data were fitted using the 4-parameter logistic fit option of GraphPad Prism 5.

Cell Culture and Proliferative Assays Using HL-60, TK 10, 786-0, M14, and MCF-7 cells. The cells were grown in RPMI 1640 Glutamax with 10% FCS, 100 μg/mL streptomycin, and 100 U/mL penicillin G and incubated in a 5% CO_2 humidified atmosphere at 37 °C. For proliferation experiments, cells were seeded in 20 μL pro well into 384-well Greiner 384 CellStar plates (Greiner Bio-One I. AG, Kremsmünster, AT). In addition to the test plates, one plate was prepared for the reference measurement at day zero. All plates were incubated for 24 h at 37 °C in a humidified atmosphere with 5% CO_2. Compounds that were dissolved in 100% DMSO (v/v) were added to test plates using the Echo 550 Liquid Handler (Labcyte Inc., Sunnyvale, UK). The final DMSO concentration in the assay was 0.5% (v/v). The viability of the cells in the day zero control plates were determined on the same day without adding any compounds. The CellTiter-Glo Viability Assay was used to determine the viability of cells using the standard protocol for this assay (Promega Corp., Madison, US). The luminescence signal was measured at the EnSpire Multimode Plate Reader (PerkinElmer, Waltham, US). Test plates were incubated for further 48 h, and the cell viability was defined as just described. Measured raw data were converted into percent of cell growth by using the high control (0.5% DMSO (v/v) without compound) and the day zero control. For dose−response studies, 11 different concentrations of compounds were tested in quadruplicates. The IC_{50} values were calculated using the 4-parameter logistic fit option of GraphPad Prism 5.

■ ASSOCIATED CONTENT

Ⓢ Supporting Information

Details of WaterMap calculation, spectroscopic details, IR data, purity and X-ray analysis for compounds, selectivity profile of **38**, measurement of intracellular uptake, and Western blot analysis. This material is available free of charge via the Internet at http://pubs.acs.org.

■ AUTHOR INFORMATION

Corresponding Author

*(C.P.) Tel: 0049 431 880 1137. Fax: 0049 431 880 1352. E-mail: cpeifer@pharmazie.uni-kiel.de.

Author Contributions

‖R.H. and B.P. contributed equally to this work. The manuscript was written through contributions of all authors. All authors have given approval to the final version of the manuscript.

Notes

The authors declare no competing financial interest.

■ ACKNOWLEDGMENTS

We thank Martin Schütt and Dr. Ulrich Girreser for excellent technical and analytical assistance at the Institute of Pharmacy in Kiel, Germany. We gratefully acknowledge the help of Dr. Dieter Schollmeyer, University of Mainz, Institute for Organic Chemistry, Germany, for X-ray analysis of compounds. Financial support by DFG grant (PE 1605/2-1) is greatly acknowledged.

■ ABBREVIATIONS USED

ADME, adsorption, distribution, metabolism, excretion; AKT1, v-akt murine thymoma viral oncogene homologue 1 (PKB); ARK5, AMPK-related protein kinase 5 (NUAK1); aurora, aurora kinase; B-RAF, v-raf murine sarcoma viral oncogene homologue B1; CDI, carbonyldiimidazole; CDK, cyclin-dependent kinase; COT, mitogen-activated protein kinase kinase kinase 8 (MAP3K8); DDQ, 2,3-dichloro-5,6-dicyano-1,4-benzoquinone; DFG-in/out, sequence motif of aspartic acid-phenylalanine-glycine of a loop in the PK domain; DMSO, dimethyl sulfoxide; EGF-R, epidermal growth factor receptor;

EPHB, EPH receptor B; FAK, focal adhesion kinase; FLT3, fms-related tyrosine kinase 3; HPI, hydrophobic pocket I; HRII, hydrophobic region II; IGF1-R, insulin-like growth factor 1 receptor; INS-R, insulin receptor; MET, met proto-oncogene (hepatocyte growth factor receptor); PDGF-R, platelet-derived growth factor receptor; PK, protein kinase; PLK1, polo-like kinase 1; RTK, receptor tyrosine kinase; SAK, serine/threonine-protein kinase (PLK4); smKI, small molecule kinase inhibitor; SRC, v-src sarcoma (Schmidt−Ruppin A-2) viral oncogene homologue; TIE2, tunica interna endothelial cell kinase; VEGF-R, vascular endothelial growth factor receptor

REFERENCES

(1) Pinchuk, B.; Johannes, E.; Gul, S.; Schlosser, J.; Schaechtele, C.; Totzke, F.; Peifer, C. Marine derived hamacanthins as lead for the development of novel PDGF-Rbeta protein kinase inhibitors. *Marine Drugs* **2013**, *11*, 3209−23.

(2) Zoraghi, R.; Worrall, L.; See, R. H.; Strangman, W.; Popplewell, W. L.; Gong, H. S.; Samaai, T.; Swayze, R. D.; Kaur, S.; Vuckovic, M.; Finlay, B. B.; Brunham, R. C.; McMaster, W. R.; Davies-Coleman, M. T.; Strynadka, N. C.; Andersen, R. J.; Reiner, N. E. Methicillin-resistant *Staphylococcus aureus* (MRSA) pyruvate kinase as a target for bis-indole alkaloids with antibacterial activities. *J. Biol. Chem.* **2011**, *286*, 44716−44725.

(3) Caldwell, J. J.; Veillard, N.; Collins, I. Design and synthesis of 2(1*H*)-pyrazinones as inhibitors of protein kinases. *Tetrahedron* **2012**, *68*, 9713−9728.

(4) Ibrahim, N.; Yu, Y.; Walsh, W. R.; Yang, J. L. Molecular targeted therapies for cancer: sorafenib mono-therapy and its combination with other therapies. *Oncology Rep.* **2012**, *27*, 1303−11.

(5) Hicken, E. J.; Marmsater, F. P.; Munson, M. C.; Schlachter, S. T.; Robinson, J. E.; Allen, S.; Burgess, L. E.; DeLisle, R. K.; Rizzi, J. P.; Topalov, G. T.; Zhao, Q.; Hicks, J. M.; Kallan, N. C.; Tarlton, E.; Allen, A.; Callejo, M.; Cox, A.; Rana, S.; Klopfenstein, N.; Woessner, R.; Lyssikatos, J. P. Discovery of a novel class of imidazo[1,2-a]pyridines with potent PDGFR activity and oral bioavailability. *Med. Chem. Lett.* **2014**, *5*, 78−83.

(6) (a) Fabbro, D.; Cowan-Jacob, S. W.; Mobitz, H.; Martiny-Baron, G. Targeting cancer with small-molecular-weight kinase inhibitors. *Methods Mol. Biol.* **2012**, *795*, 1−34. (b) Jänne, P. A.; Gray, N.; Jeff Settleman, J. Chemical structures and known kinase targets for clinically approved kinase inhibitors. *Nat. Rev. Drug Discovery* **2009**, *8*, 709−723. (c) http://www.nlm.nih.gov/cgi.

(7) Peifer, C.; Selig, R.; Kinkel, K.; Ott, D.; Totzke, F.; Schachtele, C.; Heidenreich, R.; Rocken, M.; Schollmeyer, D.; Laufer, S. Design, synthesis, and biological evaluation of novel 3-aryl-4-(1*H*-indole-3yl)-1,5-dihydro-2*H*-pyrrole-2-ones as vascular endothelial growth factor receptor (VEGF-R) inhibitors. *J. Med. Chem.* **2008**, *51*, 3814−24.

(8) Johannes, E.; Horbert, R.; Schlosser, J.; Schmidt, D.; Peifer, C. Effective synthesis of 3,5-diaryl-(1*H*)-pyrazin-2-ones via microwave mediated ring closure. *Tetrahedron Lett.* **2013**, *54*, 4067−4072.

(9) (a) Dar, A. C.; Shokat, K. M. The evolution of protein kinase inhibitors from antagonists to agonists of cellular signaling. *Annu. Rev. Biochem.* **2011**, *80*, 769−795. (b) Iwata, H.; Oki, H.; Okada, K.; Takagi, T.; Tawada, M.; Miyazaki, Y.; Imamura, S.; Hori, A.; Lawson, J. D.; Hixon, M. S.; Kimura, H.; Miki, H. A back-to-front fragment-based drug design search strategy targeting the DFG-out pocket of protein tyrosine kinases. *ACS Med. Chem. Lett.* **2012**, *3*, 342−346.

(10) Hodous, B. L.; Geuns-Meyer, S. D.; Hughes, P. E.; Albrecht, B. K.; Bellon, S.; Bready, J.; Caenepeel, S.; Cee, V. J.; Chaffee, S. C.; Coxon, A.; Emery, M.; Fretland, J.; Gallant, P.; Gu, Y.; Hoffman, D.; Johnson, R. E.; Kendall, R.; Kim, J. L.; Long, A. M.; Morrison, M.; Olivieri, P. R.; Patel, V. F.; Polverino, A.; Rose, P.; Tempest, P.; Wang, L.; Whittington, D. A.; Zhao, H. L. Evolution of a highly selective and potent 2-(pyridin-2-yl)-1,3,5-triazine tie-2 kinase inhibitor. *J. Med. Chem.* **2007**, *50*, 611−626.

(11) Cowan-Jacob, S. W.; Fendrich, G.; Floersheimer, A.; Furet, P.; Liebetanz, J.; Rummel, G.; Rheinberger, P.; Centeleghe, M.; Fabbro, D.; Manley, P. W. Structural biology contributions to the discovery of drugs to treat chronic myelogenous leukaemia. *Acta Crystallogr., Sect. D: Biol. Crystallogr.* **2007**, *63*, 80−93.

(12) Mol, C. D.; Dougan, D. R.; Schneider, T. R.; Skene, R. J.; Kraus, M. L.; Scheibe, D. N.; Snell, G. P.; Zou, H.; Sang, B. C.; Wilson, K. P. Structural basis for the autoinhibition and STI-571 inhibition of c-Kit tyrosine kinase. *J. Biol. Chem.* **2004**, *279*, 31655−63.

(13) Getlik, M.; Grutter, C.; Simard, J. R.; Kluter, S.; Rabiller, M.; Rode, H. B.; Robubi, A.; Rauh, D. Hybrid compound design to overcome the gatekeeper T338M mutation in cSrc. *J. Med. Chem.* **2009**, *52*, 3915−3926.

(14) Harris, P. A.; Boloor, A.; Cheung, M.; Kumar, R.; Crosby, R. M.; Davis-Ward, R. G.; Epperly, A. H.; Hinkle, K. W.; Hunter, R. N., III; Johnson, J. H.; Knick, V. B.; Laudeman, C. P.; Luttrell, D. K.; Mook, R. A.; Nolte, R. T.; Rudolph, S. K.; Szewczyk, J. R.; Truesdale, A. T.; Veal, J. M.; Wang, L.; Stafford, J. A. Discovery of 5-[[4-[(2,3-dimethyl-2*H*-indazol-6-yl)methylamino]-2-pyrimidinyl]amino]-2-methyl-b enzenesulfonamide (Pazopanib), a novel and potent vascular endothelial growth factor receptor inhibitor. *J. Med. Chem.* **2008**, *51*, 4632−40.

(15) Hilberg, F.; Roth, G. J.; Krssak, M.; Kautschitsch, S.; Sommergruber, W.; Tontsch-Grunt, U.; Garin-Chesa, P.; Bader, G.; Zoephel, A.; Quant, J.; Heckel, A.; Rettig, W. J. BIBF 1120: triple angiokinase inhibitor with sustained receptor blockade and good antitumor efficacy. *Cancer Res.* **2008**, *68*, 4774−82.

(16) Meyers, M. J.; Pelc, M.; Kamtekar, S.; Day, J.; Poda, G. I.; Hall, M. K.; Michener, M. L.; Reitz, B. A.; Mathis, K. J.; Pierce, B. S.; Parikh, M. D.; Mischke, D. A.; Long, S. A.; Parlow, J. J.; Anderson, D. R.; Thorarensen, A. Structure-based drug design enables conversion of a DFG-in binding CSF-1R kinase inhibitor to a DFG-out binding mode. *Bioorg. Med. Chem. Lett.* **2010**, *20*, 1543−7.

(17) (a) Jacobson, M. P.; Kaminski, G. A.; Friesner, R. A.; Rapp, C. S. Force field validation using protein side chain prediction. *J. Phys. Chem. B* **2002**, *106*, 11673−11680. (b) Jacobson, M. P.; Pincus, D. L.; Rapp, C. S.; Day, T. J. F.; Honig, B.; Shaw, D. E.; Friesner, R. A. A hierarchical approach to all-atom protein loop prediction. *Proteins: Struct., Funct., Bioinf.* **2004**, *55*, 351−367.

(18) Friesner, R. A.; Banks, J. L.; Murphy, R. B.; Halgren, T. A.; Klicic, J. J.; Mainz, D. T.; Repasky, M. P.; Knoll, E. H.; Shelley, M.; Perry, J. K.; Shaw, D. E.; Francis, P.; Shenkin, P. S. Glide: A new approach for rapid, accurate docking and scoring. 1. Method and assessment of docking accuracy. *J. Med. Chem.* **2004**, *47*, 1739−1749.

(19) (a) Abel, R.; Young, T.; Farid, R.; Berne, B. J.; Friesner, R. A. Role of the active-site solvent in the thermodynamics of factor Xa ligand binding. *J. Am. Chem. Soc.* **2008**, *130*, 2817−2831. (b) Young, T.; Abel, R.; Kim, B.; Berne, B. J.; Friesner, R. A. Motifs for molecular recognition exploiting hydrophobic enclosure in protein-ligand binding. *Proc. Natl. Acad. Sci. U.S.A.* **2007**, *104*, 808−13. (c) Haider, K.; Huggins, D. J. Combining solvent thermodynamic profiles with functionality maps of the Hsp90 binding site to predict the displacement of water molecules. *J. Chem. Inf. Modeling* **2013**, *53*, 2571−86. (d) Snyder, P. W.; et al. Mechanism of the hydrophobic effect in the biomolecular recognition of arylsulfonamides by carbonic anhydrase. *Proc. Natl. Acad. Sci. U.S.A.* **2011**, *108*, 17889−17894. (e) Breiten, B.; et al. Water networks contribute to enthalpy/entropy compensation in protein-ligand binding. *J. Am. Chem. Soc.* **2013**, *135*, 15579−15584.

(20) (a) Robinson, D. D.; Sherman, W.; Farid, R. Understanding kinase selectivity through energetic analysis of binding site waters. *ChemMedChem* **2010**, *5*, 618−27. (b) Myrianthopoulos, V.; Kritsanida, M.; Gaboriaud-Kolar, N.; Magiatis, P.; Ferandin, Y.; Durieu, E.; Lozach, O.; Cappel, D.; Soundararajan, M.; Filippakopoulos, P.; Sherman, W.; Knapp, S.; Meijer, L.; Mikros, E.; Skaltsounis, A. L. Novel inverse binding mode of indirubin derivatives yields improved selectivity for DYRK kinases. *ACS Med. Chem. Lett.* **2013**, *4*, 22−26.

(21) Abad-Zapatero, C. Ligand efficiency indices for effective drug discovery. *Expert Opin. Drug Discovery* **2007**, *2*, 469−88.

(22) Furet, P.; Bold, G.; Meyer, T.; Roesel, J.; Guagnano, V. Aromatic interactions with phenylalanine 691 and cysteine 828: a concept for FMS-like tyrosine kinase-3 inhibition. Application to the

discovery of a new class of potential antileukemia agents. *J. Med. Chem.* **2006**, *49*, 4451−4454.
(23) Reiterer, G.; Yen, A. Platelet-derived growth factor receptor regulates myeloid and monocytic differentiation of HL-60 cells. *Cancer Res.* **2007**, *67*, 7765−72.
(24) Riley, H. L. Oxidation Activity of Selenium Dioxide. *Nature* **1947**, *159*, 571−572.
(25) (a) Schwering, U. Dissertation, University of Kiel; http://macau.uni-kiel.de/receive/dissertation_diss_00005345. (b) Fogh, J.; Fogh, J. M.; Orfeo, T. One hundred and twenty-seven cultured human tumor cell lines producing tumors in nude mice. *J. Natl. Cancer Inst.* **1977**, *59*, 221−226.
(26) Servidei, T.; Riccardi, A.; Sanguinetti, M.; Dominici, C.; Riccardi, R. Increased sensitivity to the platelet-derived growth factor (PDGF) receptor inhibitor STI571 in chemoresistant glioma cells is associated with enhanced PDGF-BB-mediated signaling and STI571-induced Akt inactivation. *J. Cell. Physiol.* **2006**, *208*, 220−228.
(27) Delepine, M. Sur l'hexaméthylene-amines; seld dámmonium; action des acides; production d'amines primaires. *C. R. Hebd. Seances Acad. Sci.* **1895**, *120*, 501−502.
(28) Suzuki, M.; Iwasaki, T.; Miyoshi, M.; Okumura, K.; Matsumot, K. Synthesis of amino-acids and related compounds. New convenient syntheses of alpha-C-acylamino acids and alpha-amino ketones. *J. Org. Chem.* **1973**, *38*, 3571−3575.
(29) Halgren, T. A.; Murphy, R. B.; Friesner, R. A.; Beard, H. S.; Frye, L. L.; Pollard, W. T.; Banks, J. L. Glide: A new approach for rapid, accurate docking and scoring. 2. Enrichment factors in database screening. *J. Med. Chem.* **2004**, *47*, 1750−1759.
(30) Jacobson, M. P.; Friesner, R. A.; Xiang, Z. X.; Honig, B. On the role of the crystal environment in determining protein side-chain conformations. *J. Mol. Biol.* **2002**, *320*, 597−608.
(31) (a) Lazaridis, T. Inhomogeneous fluid approach to solvation thermodynamics. 1. Theory. *J. Phys. Chem. B* **1998**, *102*, 3531−3541. (b) Lazaridis, T. Inhomogeneous fluid approach to solvation thermodynamics. 2. Applications to simple fluids. *J. Phys. Chem. B* **1998**, *102*, 3542−3550.